Quantum Electronics **47** (3) 236–244 (2017)

https://doi.org/10.1070/QEL16299

A method for measuring the amplitude and phase of ultrashort laser pulses using self-modulation in a Kerr medium and spectral interferometry

A.V. Andrianov, A.V. Kim, E.A. Khazanov

Abstract. **A new method is proposed for measuring the field of ultrashort pulses by assessing spectral interference between an input pulse and the pulse transmitted through a Kerr medium. The proposed iterative algorithm allows the pulse amplitude and phase to be reconstructed. Our numerical experiments demonstrate that the proposed algorithm can be used to reconstruct pulses with complex intensity and phase shapes and is stable to a noise in input data. The method requires that only one nonlinear element be placed in the laser beam to be studied.**

Keywords: *measuring the field of ultrashort pulses, self-modulation, spectral interference, iterative algorithms.*

1. Introduction

The metrology of ultrashort optical pulses remains a topical issue in laser physics, even though it has been the subject of intense studies in the past few decades [1]. Interest in this area of research is aroused, in particular, by the fact that parameters of pulses generated by state-of-the-art laser systems reach extreme values: ultralarge spectral bandwidth and ultrashort duration. Moreover, pulse parameters often lie in spectral regions poorly explored from the viewpoint of the physics of ultrashort pulses (USPs), where existing methods are difficult to apply. In addition, an important aspect of USP measurements, which is currently the subject of intense discussion, is the ability to obtain a complete spatiotemporal information about an optical beam, which in fact requires that the temporal pulse shape be measured at each point in its cross section [2]. This issue is of particular current interest for ultrahigh power laser systems and experiments on nonlinear interaction between ultra-intense laser radiation and matter. In this respect, particularly promising are single-pulse techniques for measuring the shape of an ultrashort pulse and techniques that are easy to adapt to simultaneous measurements at many points in the cross section of a beam.

Complete characterisation of a USP requires knowledge of not only the temporal shape of its intensity but the temporal shape of its phase. Among widely used approaches that allow such information to be extracted from experimental measurements and require no known reference pulse, it is worth noting frequency-resolved optical gating (FROG) methods [3, 4] and methods based on spectral phase retrieval from spectral interferometry data. These latter include spectral phase interferometry for direct electric-field reconstruction (SPIDER) of USPs [5], a method based on the observation of spectral interference between two frequency-shifted replicas of an object pulse and having a direct pulse shape reconstruction algorithm and approaches in which a reference pulse is generated from an object pulse using a nonlinear process [self-referenced spectral interferometry (SRSI) [6]], such as cross-polarised wave (XPW) generation [7]. Less widespread are techniques that employ autocorrelation measurements with additional spectral or interference measurements and the corresponding iterative algorithms for solving the inverse problem [8].

There is independent interest in methods based on measurements of the spectrum of a pulse (here and in what follows, we mean measurements of the magnitude of a spectrum) after it has passed through a medium with third-order (Kerr) nonlinearity. Spectra of such pulses depend significantly on their initial spectral phase [9]. A method proposed by Nibbering et al. [10] and further developed by Ferreiro et al. [11] attracted little attention for a long time, because its applicability is subject to significant limitations. Recent work by Anashkina et al. [12] has demonstrated that, using an additional, third measurement of the spectrum of a pulse, after it has passed through a medium with a different Kerr nonlinearity value or a different thickness, the application area of the method can be considerably extended. The method was successfully used to measure the pulse shape in an ultrahigh-power parametric system [12] with thin plastic films as third-order nonlinear medium. One advantage of this method is that it is relatively easy to implement experimentally in the case of a high-power laser system with an intensity at a level of $\sim$1 TW cm^{-2} or more in a single-pulse mode. Unfortunately, the necessity of taking the spectrum at two thicknesses of the nonlinear medium hinders the use of this method for measuring pulse characteristics in the cross section of a beam.

In this work, we propose a new method of USP measurements which requires only one nonlinear element in a laser beam under study. The method is rather easy to adapt to simultaneous measurements at many points in the cross section of the beam.

2. Idea of the measurement method

The principle proposed in this study for measuring the amplitude and phase of USPs is as follows. One measures three spectra: the spectrum of a pulse before it passes through a nonlinear medium, its spectrum after it passes through a non-

A.V. Andrianov, A.V. Kim, E.A. Khazanov Institute of Applied Physics, Russian Academy of Sciences, ul. Ul'yanova 46, 603950 Nizhnii Novgorod, Russia; e-mail: alex.v.andrianov@gmail.com

Received 6 February 2017
Kvantovaya Elektronika **47** (3) 236–244 (2017)
Translated by O.M. Tsarev

linear (Kerr) medium and the spectrum of the coherent sum of the two pulses. From these spectra, an algorithm reconstructs the initial pulse field. This method differs from those above in that it includes an additional observation of spectral interference between an input pulse and the pulse transmitted through a nonlinear medium, which allows one to subsequently gain information about the variation in the spectral phase of the pulse as it passes through the nonlinear element.

Figure 1 schematically illustrates the proposed configuration for the practical implementation of the method, convenient for performing experiments in systems operating in a single-pulse mode. A high-power light beam is directed to a thin plate of a nonlinear material at a small angle to the normal. The signals reflected from the front and back faces of the plate are sent to a spectrometer to observe spectral interference. The signal reflected from the back face has a considerably lower intensity (~4% at typical refractive indices) than the input signal, so the effect of nonlinearity during the backward pass of the signal through the plate can be neglected. The three spectra in question can be measured by either three spectrographs or one if the three beams will be separated in a plane normal to the plane of Fig. 1.

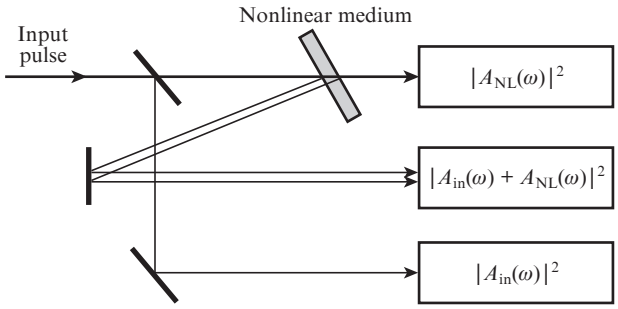

Figure 1. Schematic configuration for measuring the field of ultrashort pulses.

At a good visibility of the spectral interference pattern, the three spectra can be retrieved from two measurements (of the output spectrum and spectral interference), which makes the proposed method one of the easiest to implement experimentally: in fact, the setup comprises one nonlinear element and a spectrometer.

The proposed configuration is in principle suitable for measuring the input, transformed and interference spectra at the same point in a cross section of the beam, which may be important for characterising spatiotemporal distortions. If two-dimensional photodetector arrays (cameras) are used as recording elements in the spectrometers, one can obtain a set of spectra in a single-pulse mode along a line parallel to the spectrometer slit. This offers the possibility of further reconstructing the temporal shape along the line chosen in a cross section of the beam.

3. Pulse shape reconstruction algorithm

Let the field of a pulse at the input of a nonlinear medium have the form $E(x,y,z,t) = \mathrm{Re}\,(A_{in}(t))\exp(-i\omega_0 t)$, where $A_{in}(t)$ is the complex envelope and ω_0 is the carrier frequency. We introduce the forward and inverse Fourier transform operators as follows:

$$\hat{F}[A] = \frac{1}{\sqrt{2\pi}}\int_{-\infty}^{+\infty} A(t)\exp(i\omega t)\,dt, \tag{1}$$

$$\hat{F}^{-1}[A] = \frac{1}{\sqrt{2\pi}}\int_{-\infty}^{+\infty} A(\omega)\exp(-i\omega t)\,dt. \tag{2}$$

The experimentally measured spectrum of the input signal can then be written in the form

$$S_0(\omega) = |F[A_{in}]|^2. \tag{3}$$

While travelling through a medium with Kerr nonlinearity, the pulse acquires an additional phase in the time domain due to the self-phase modulation effect. The complex envelope of the pulse at the output of the nonlinear medium has the form [13]

$$A_{NL}(t) = A_{in}(t)\exp(i\gamma d|A_{in}(t)|^2), \tag{4}$$

where γ is the nonlinearity coefficient of the medium and d is the thickness of the plate. The maximum shift of the nonlinear phase as the pulse passes through the nonlinear medium is characterised by the value of the B-integral:

$$B = \int_0^d \gamma|A_{max}|^2\,dz = \gamma d|A_{max}|^2, \tag{5}$$

where $|A_{max}|^2$ is the peak signal intensity.

The experimentally measured spectral intensity at the output of the nonlinear medium is

$$S_1(\omega) = |F[A_{NL}]|^2. \tag{6}$$

It should be emphasised that neither the input signal peak intensity $|A_{max}|^2$, nor the nonlinearity coefficient γ nor their product is presupposed to be known. Dispersion effects and higher order nonlinear effects will be neglected, and we will assume that the nonlinear medium is sufficiently thin and that the spectrum is not very broad.

The spectral intensity of the coherent sum of the signals at the input and output of the nonlinear medium has the form

$$S_{01}(\omega) = |F[A_{in}] + F[A_{NL}(t+\tau)]|^2. \tag{7}$$

Here we take into account that the signal arriving at the spectrometer from the output of the nonlinear medium has a time delay $\tau = 2nd/c$ relative to the input signal, where n is the refractive index of the plate and c is the speed of light.

The problem of reconstructing the shape of the pulse under consideration can now be formulated as follows: from known S_0, S_1 and S_{01} spectra, we should find such a complex envelope of the input field $A_{in}(t)$ that relations (3), (4), (6) and (7) are fulfilled for some value of the $\gamma d|A_{max}|^2$ product. At the present stage, we do not know whether this inverse problem can be solved directly; nevertheless, such problems can be successfully solved using various iterative algorithms.

The first step – determination of the difference between the spectral phases at the input and output of the nonlinear medium, $\phi(\omega) = \arg(F[A_{NL}]) - \arg(F[A_{in}])$ – can be performed using a direct algorithm that has been discussed many times in relation to problems of spectral interferometry [1, 6]. The algorithm is based on separating out the rapidly oscillating component of an interference spectrum using the inverse

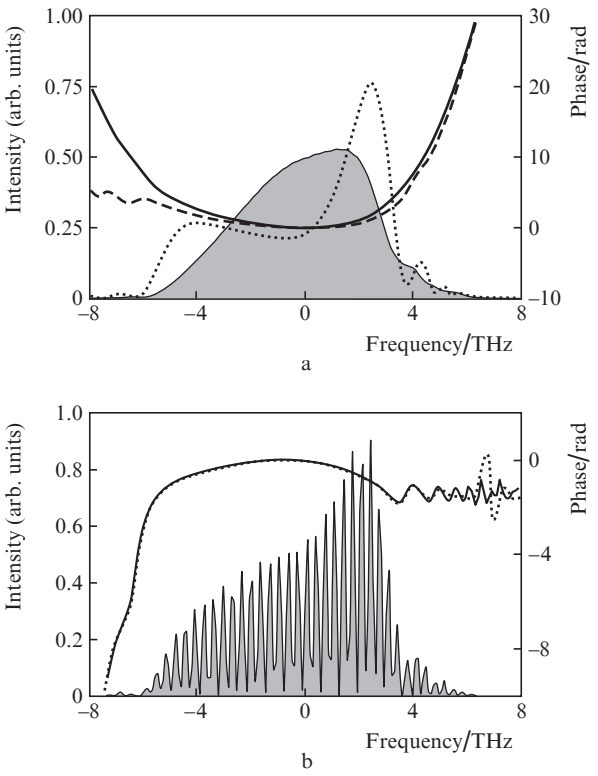

Figure 2. (a) Spectrum (shaded area) and phase (solid line) of a pulse at the input of a nonlinear medium and spectrum (dotted line) and phase (dashed line) at the output of the nonlinear medium; (b) interference spectrum (shaded area) and phase difference $\phi(\omega)$ obtained by direct calculation (solid line) and extracted from the interference spectrum (dotted line).

Fourier transformation to the time domain $S_{01}(t) = F^{-1}[S_{01}(\omega)]$, the filtering off of the component in the time interval around τ, the forward Fourier transformation of the filtered signal $S'_{01}(t)$ to the frequency domain $S'_{01}(\omega) = F[S'_{01}(t)]$ and phase retrieval from the resultant complex function. The phase retrieval from an interference spectrum is exemplified in Fig. 2.

Further, to find an approximate solution to the problem of reconstructing the pulse shape, we propose an iterative algorithm schematised in Fig. 3. The algorithm employs principles basic to iterative algorithms for phase reconstruction from frequency-domain and time-domain intensity data, such as the Gerchberg–Saxton algorithm [14].

The operation of the algorithm begins in step 1. In the first iteration, an initial conjecture as to the complex spectrum of the pulse at the output of the nonlinear medium, $A_0(\omega)$, e.g. a noise signal with a random spectral phase, is fed to its input. Below, we will explain why the output signal, rather than the input one, is chosen as the starting point. In step 1, the magnitude of the spectrum is replaced by the experimentally measured spectrum $\sqrt{S_1}$, without changing the spectral phase. The resultant complex spectrum is fed to the input of step 2. In addition, the time-domain signal $A_1(t)$ obtained by inverse Fourier transformation is sent to input of steps 5 and 3. Step 2 uses information about the measured difference between the spectral phases of the signal before and after it passed through the nonlinear medium, $\phi(\omega)$, and information about the measured magnitude of the spectrum at the input of the nonlinear medium, S_0. After step 2, the complex spectrum of the signal at the input of the nonlinear medium, $A_2(t)$, is computed. The spectral bandwidth of the input signal is typically smaller than that of the output signal, so the effect of inaccurate spectral phase determination, especially at the edges of the spectrum, becomes reduced in step 2. It is for this reason that the broadest spectrum is taken as the starting point of the algorithm. If the output spectrum is narrower than the input one (e.g. when the input pulse has a corresponding phase), the algorithm can readily be modified by replacing S_0 with S_1, ϕ with $-\phi$ and γ with $-\gamma$.

Steps 3 and 4 are used to take into account the nonlinear propagation of the signal. In step 3, backward propagation from the output to the input is modelled by adding a proper time-domain phase (4), and in step 4 the amplitude of the resultant spectrum is replaced by the experimentally measured one, $\sqrt{S_0}$. Since the nonlinearity of the medium is supposed to be unknown, it can be adjusted in each iteration in the simplest implementation of the algorithm. This can be done via several passes of steps 3 and 4 at different test nonlinearity values, γd. The best of them is the one minimising the discrepancy between resultant spectrum $|A_3(\omega)|^2$ and the experimentally measured spectrum S_0.

In step 5, the time-domain shape of the pulse intensity profile is corrected. In doing so, use is made of the fact that the pulse intensity profile should be the same at the input and output of the nonlinear medium: $|A_1(t)| = |A_2(t)|$ [see rela-

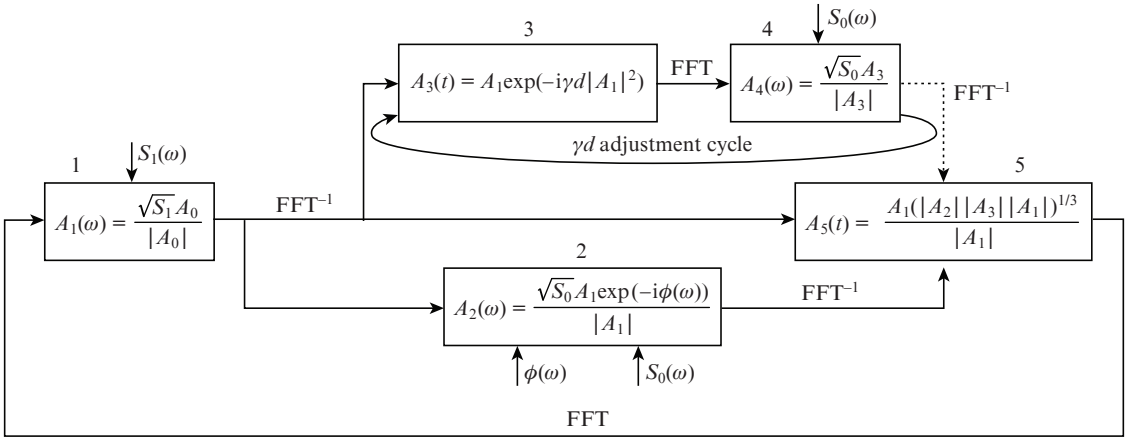

Figure 3. Flow chart of the iterative pulse shape reconstruction algorithm; FFT and FFT^{-1} are forward and inverse fast Fourier transformations.

tion (4)]. Moreover, in the case of the convergence to the correct solution, the intensity profile obtained in step 4 should also coincide with this profile: $|A_3(t)| = |A_1(t)| = |A_2(t)|$. As the corrected intensity profile, the geometric mean of the intensities $(|A_1(t)||A_2(t)||A_3(t)|)^{1/3}$ was chosen for the next iteration. This choice ensured good results with various test pulse shapes. Nevertheless, other functions, such as the arithmetic mean, including the one with various weighting schemes, may occasionally ensure better results.

The convergence of the algorithm to the correct solution was verified by computing the discrepancy between the reconstructed spectral intensities $A_1(\omega)$ and $A_3(\omega)$ and the experimentally measured S_0 and S_1, as well as the discrepancy between the reconstructed pulse envelopes at the input and output of the nonlinear medium, $A_1(t)$ and $A_2(t)$:

$$\Delta_0 = \frac{\| S_0(\omega) - |A_1(\omega)|^2 \|^{1/2}}{\| \sqrt{S_0(\omega)} \|},$$

$$\Delta_1 = \frac{\| S_1(\omega) - |A_0(\omega)|^2 \|^{1/2}}{\| \sqrt{S_1(\omega)} \|}, \qquad (8)$$

$$\Delta_2 = \frac{\| |A_1(t)|^2 - |A_2(t)|^2 \|^{1/2}}{\| A_1(t) \|},$$

where

$$\|f\| = \sum_{j=1}^{N} |f_j|^2,$$

and N is the number of grid points in the time domain (and frequency domain). The algorithm minimises the dimensionless discrepancy $\Delta = \Delta_0 + \Delta_1 + \Delta_2$, which tends to zero as the correct solution is approached.

An interesting feature of the algorithm is that, for many test pulse shapes, the correct solution can be found without using the 'nonlinear branch' (steps 3 and 4). In such a case, the operation of the algorithm was essentially based on the

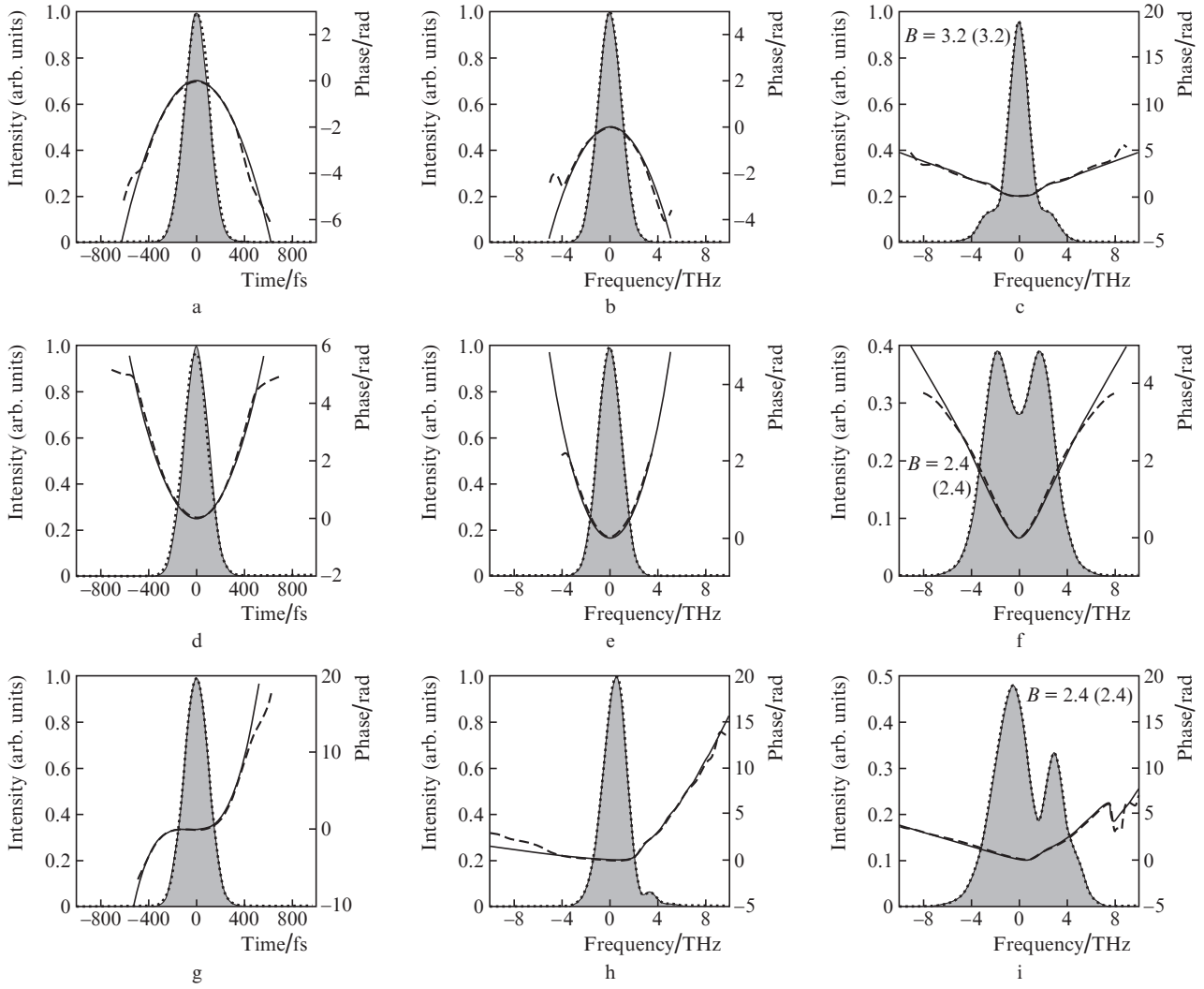

Figure 4. Reconstruction algorithm results for test pulses with various time-domain phase parameters: (a–c) quadratic phase, $\alpha = -2$ ps^{-2}; (d–f) quadratic phase, $\alpha = 2$ ps^{-2}; (g–i) cubic phase, $\beta = 100$ ps^{-3}. The plots represent (a, d, g) time-domain intensity and phase distributions, (b, e, h) spectra and spectral phases at the input of the nonlinear medium and (c, f, i) spectra and spectral phases at the output of the nonlinear medium. The following notation is used: the shaded areas represent the parent intensity profiles, the dotted lines are the reconstructed intensity profiles, the solid lines represent the initial phase, and the dashed lines represent the reconstructed phase. Figures 4c, 4f and 4i specify the B-integral for the spectra at the output of the nonlinear medium (the numbers in round brackets are the reconstructed values).

requirement that the pulse intensity profiles at the input and output of the nonlinear medium be identical, without using relation (4) for the time-domain phase, and the discrepancy to be minimised was $\Delta_0 + \Delta_2$. Most likely, in this implementation the problem may occasionally have a few correct solutions or very different solutions with rather similar reconstructed spectral intensity shapes – such examples were indeed found in test computations. Nevertheless, an operation mode without 'nonlinear branch' feedback can be used to accelerate the algorithm operation in a few intermediate iterations, with periodic checks of the solution with allowance for nonlinearity. In this version, a search for the γd value is needed only in some iterations. In our implementation of the proposed algorithm, we adjusted the nonlinearity value in every fifth iteration via several passes of steps 3 and 4. The search was performed by merely trying B-integrals in the range 0.3–6 at a step size of 0.05, which, according to our observations, ensured sufficient reconstruction accuracy and a sufficient algorithm operation rate. In addition, a mechanism preventing algorithm stagnation was implemented. If the discrepancy did not decrease over

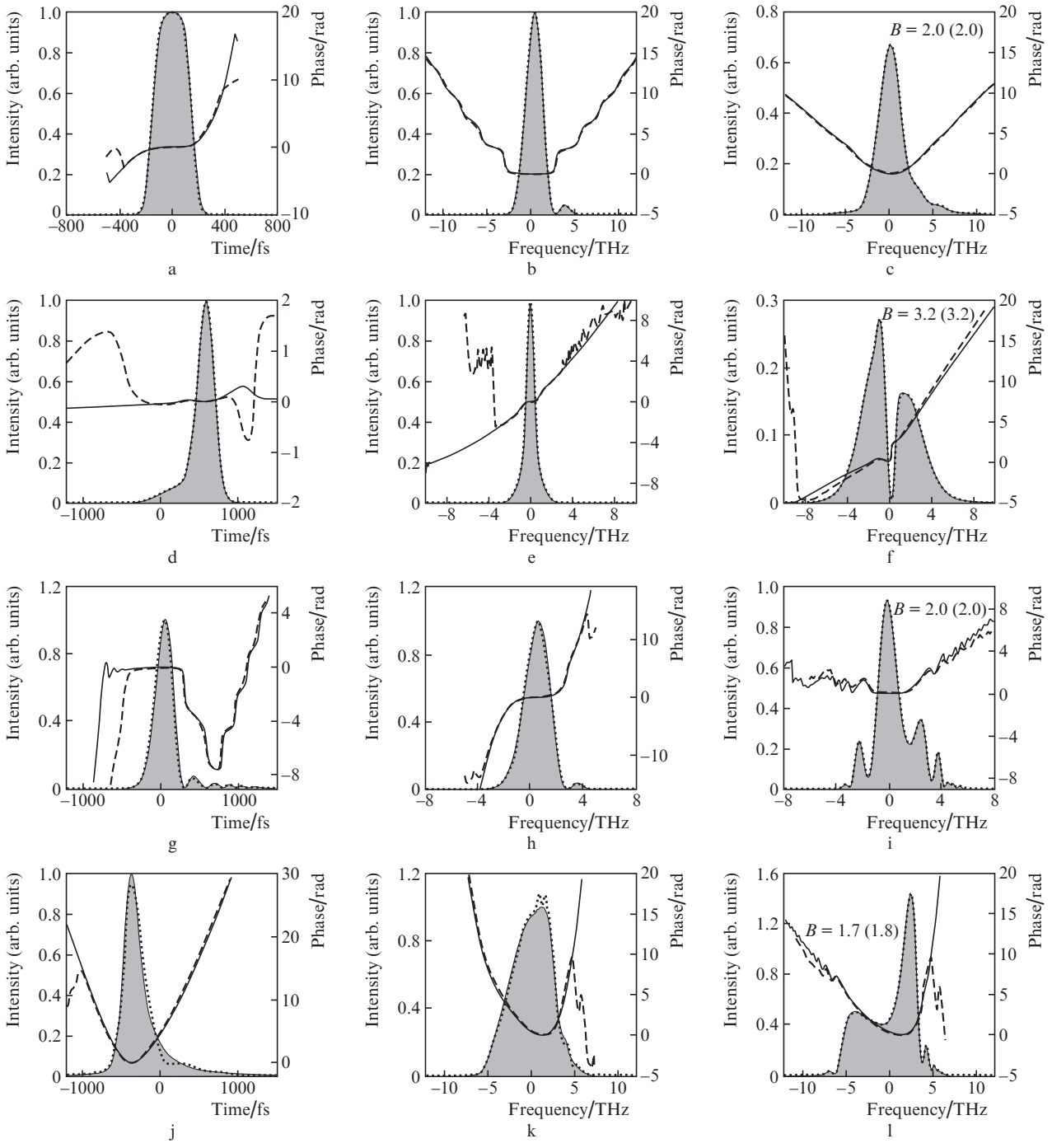

Figure 5. Reconstruction algorithm results for test pulses with a complex envelope and phase. The pulse parameters are indicated in text. Designations are the same as in Fig. 4.

150 iterations, the pulse intensity profile was replaced by the best profile found by that time, with the addition of random perturbations.

4. Numerical simulation

To verify the feasibility of using the proposed method, we carried out various numerical experiments in which we used several test shapes of input pulses, under both idealised conditions, with no noise, and nearly experimental conditions.

The choice of test pulse shapes capable of adequately revealing potential problems in the operation of reconstruction algorithms has been repeatedly discussed in analysing previously proposed methods, such as FROG [3] and spectral interferometry [15], and in searching for ambiguities in their application.

All the numerical experiments were carried out using time- and frequency-domain grids of 512 points, which corresponds to a typical resolution of IR cameras. The thickness of the plate corresponded to a time delay of 2.9 ps. Below, we pres-

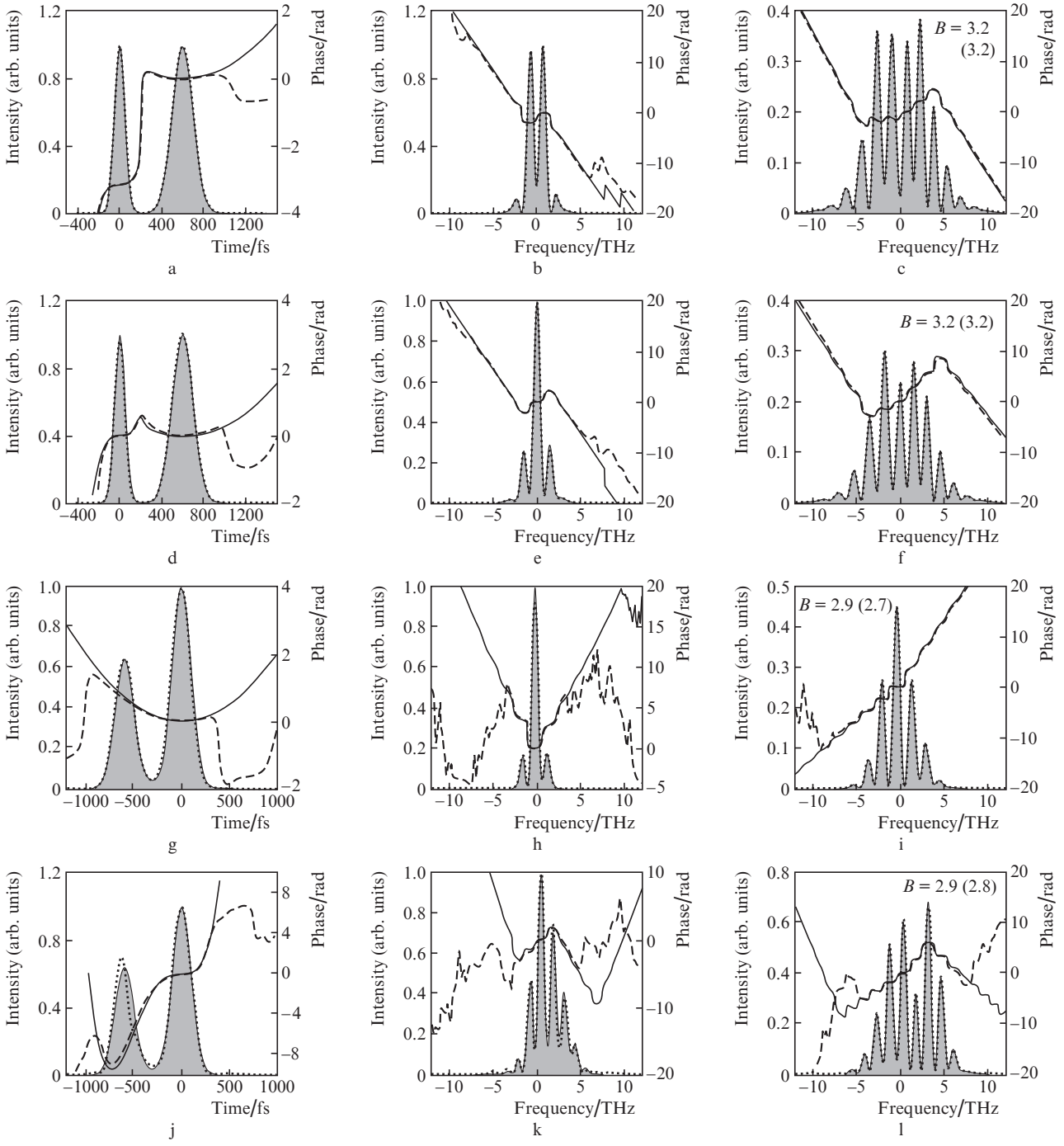

Figure 6. Reconstruction algorithm results for double test pulses. The pulse parameters are indicated in text. Designations are the same as in Figs 4 and 5.

ent the spectral phases of signals at the input and output of the nonlinear medium, rather than interference spectra, which carry no useful visual information.

The first series of numerical tests demonstrates the feasibility of reconstructing pulses with a quadratic and a cubic time-domain phase using the proposed algorithm. The complex envelope of an input pulse has the form $A(t) = \exp(-t^2/T^2 + i\alpha t^2 + i\beta t^2)$, where T is the pulse duration and α and β are coefficients of the quadratic and cubic pulse phases. Figure 4 presents algorithm operation results for pulses with various parameters. It is seen that, in all instances, both the shape and phase of the time-domain pulse envelope were reconstructed almost ideally. The spectral phases of the starting and transformed pulses were also adequately reconstructed, which suggests that the nonlinearity coefficient was properly adjusted.

Next, we tested various more complex shapes of the pulse envelope and shape. Figures 5a–5c present results for a super-Gaussian pulse with a polynomial phase $A(t) = \exp(-t^4/T^4 + i\alpha t^2 + i\beta t^3 + i\delta t^4)$, where $T = 200$ fs; $\alpha = 2$ ps^{-2}; $\beta = 100$ ps^{-3}; and $\delta = 100$ ps^{-4}. Figures 5d–5f exemplify the reconstruction of a pulse with a pedestal, which has an envelope $A(t) = a\exp(-t^2/T_1^2) + \exp[-(t - s_2)^2/T_2^2 + i\alpha(t - s_2)^2]$, where $a = 0.3$;

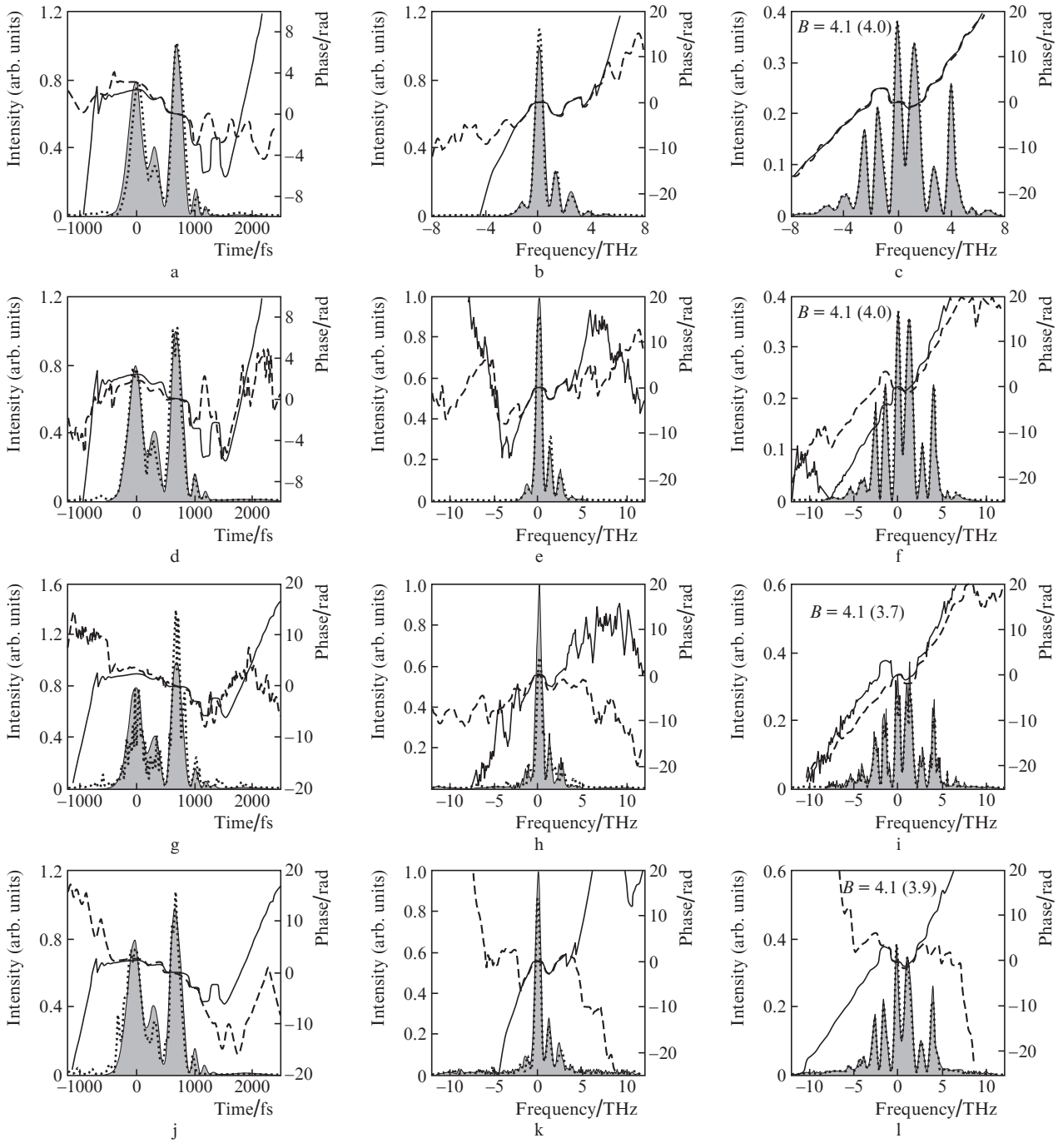

Figure 7. Reconstruction algorithm results for noisy input data. The pulse parameters are indicated in text. Designations are the same as in Figs 4–6.

T_1 = 400 fs; T_2 = 200 fs; s_2 = –400 fs; and α = 2 ps^{-2}. The example in Figs 5g–5i examines a pulse with an oscillating tail and complex phase. The starting Gaussian pulse with a polynomial phase (T = 200 fs, α = 2 ps^{-2} and β = 100 ps^{-3}) was passed through a medium with a dispersion that introduced a spectral phase of the form $\psi = \sigma\omega^2 + i\rho\omega^3$, where σ = 0.0072 ps^2 and ρ = 0.00084 ps^3. Not only the intensity profile of the oscillating pulse tail but also the complex time-domain phase were adequately reconstructed. The example in Figs 5j–5l presents an asymmetric pulse with a very long pedestal and a strong nonlinear time dependence of its phase. Owing to the special pulse and phase shapes, the spectrum of the pulse broadens rather weakly when it passes through the nonlinear medium. The intensity profile reconstruction is nonideal; nevertheless, the time-domain phase is adequately reconstructed, up to several tens of radians. Except for a small part in the high-frequency region, the spectral phases of both the input and transformed signals are adequately reconstructed. Inadequate reconstruction results are noticeable in the spectral intensity curves of the input signal. Thus, the algorithm offers the possibility of assessing the quality of the solution obtained. Characteristic $\Delta = \Delta_0 + \Delta_1 + \Delta_2$ discrepancies decrease to 10^{-7}–10^{-4} in the case of good convergence (the cases represented in Figs 5a, 5d and 5g). If the reconstruction result is nonideal, the discrepancy is at a level of 10^{-4} to 10^{-2} (Δ = 0.006 in Fig. 5j).

The above examples show successful time axis direction determination, which is impossible in the case of algorithms based on the use of quadratic nonlinearity without additional measurements (second-harmonic FROG method and autocorrelation method).

One commonly accepted test for checking algorithms of pulse shape measurements is the use of double pulses. Examples of algorithm operation with such pulses are presented in Fig. 6. Figures 6a and 6d demonstrate the ability of the algorithm to determine the absolute phase between pulses, which is a nontrivial problem for many methods. Test pulses spaced 600 fs apart were Gaussian in shape and had polynomial phases with parameters T = 100 fs, α = 0 and β = 100 ps^{-3} (first pulse) and T = 200 fs, α = 2 ps^{-2} and β = 0 (second pulse). The absolute phase between them was zero (Fig. 6d) or π (Fig. 6a).

Figures 6g–6l present reconstruction results for Gaussian pulses identical in duration (T = 200 fs) but differing in intensity (intensity ratio of 0.64). The pulses had the same polynomial phase with the following parameters: α = –2 ps^{-2} and $\beta = \delta$ = 0 (Fig. 6g) and α = –2 ps^{-2}, β = –100 ps^{-3} and δ = –100 ps^{-4} (Fig. 6l). In the latter instance, the double pulse intensity profile reconstruction is nonideal. Nevertheless, it is worth noting the adequate reconstruction of the complex T phase, which varies over more than 8 rad between pulse centres. Numerical experiments indicate that the B-integral values at which the method yields adequate results lie in the range 1.5–4.5, depending on the particular pulse shape.

Next, algorithm operation was tested under nearly typical experimental conditions. To this end, we used a rather complex test signal in the form of the sum of a few pulses differing in amplitude and phase, which was then passed through a dispersive medium. In addition, a random noise was added to the spectra at the input and output of the nonlinear medium. The reconstruction algorithm results are presented in Fig. 7. Noise was added by two procedures. In one of them, noise was added to both the real and imaginary parts of the complex spectra before taking the square of their magnitude. This may correspond to some random components of light coming together with the pulse. In the other procedure, noise was added to the squares of the magnitudes of the spectra, which corresponds to the intrinsic noise of the spectrometer and an incoherent component of light. In Figs 7a–7c, no noise is added. In Figs 7d–7f, a 1% noise is added to the complex amplitude (peak-to-peak relative to the amplitude of the $\sqrt{S_0}$ and $\sqrt{S_1}$ spectra, which corresponds to a 10% deviation at the maximum of the square of the magnitude of the spectrum). In Figs 7g–7i, a 10% noise is added to the complex envelope (which corresponds to a 30% deviation at the maximum of the square of the magnitude of the spectrum). In Figs 7j–7l, a 3% noise is added to the square of the magnitude of the spectrum. It is seen that, in all cases, the reconstruction result is nonideal. Nevertheless, even in the presence of a considerable noise component in input data, the general pulse structure is adequately reconstructed. A characteristic discrepancy is at a level of 0.01 to 0.08. Thus, the proposed algorithm is sufficiently stable even in the case of a rather complex input pulse shape, and the presence of an additional noise in input data causes no catastrophic distortion of reconstruction results.

The characteristic number of algorithm iterations after which the discrepancy does not decrease is about 100 in simple cases and increases to several thousand (usually no greater than 10 000) for complex pulses and noisy input data. A typical operating time of our program implementation of the algorithm on a personal computer with an Intel Core i5 processor (1.7 GHz) is several seconds to several minutes.

In conclusion, note that the proposed method for measuring the amplitude and phase of ultrashort pulses is based on measuring spectral interference between an input pulse and the pulse transmitted through a medium with third-order (Kerr) nonlinearity. Our numerical experiments have demonstrated that the proposed algorithm is effective in reconstructing pulses with complex intensity and phase shapes and stable to a noise in input data. The method allows for measurements in a single pulse mode and requires that only one nonlinear element be placed in the laser beam to be studied.

Acknowledgements. This work was supported by the RF Ministry of Education and Science (Project No. 14.Z50.31.0007) and the Presidium of the Russian Academy of Sciences (Programme 'Extreme laser radiation: physics and fundamental applications').

References

1. Walmsley I.A., Dorrer C. *Adv. Opt. Photonics*, **1**, 308 (2009).
2. Pariente G., Gallet V., Borot A., Gobert O., Quéré F. *Nat. Photonics*, **10**, 547 (2016).
3. Trebino R. *Frequency-Resolved Optical Gating: the Measurement of Ultrashort Laser Pulses* (Kluwer Academic, 2002).
4. Trebino R. et al. *Rev. Sci. Instrum.*, **68**, 3277 (1997).
5. Iaconis C., Walmsley I.A. *Opt. Lett.*, **23**, 792 (1998).
6. Oksenhendler T., Coudreau S., Forget N., Crozatier V., Grabielle S., Herzog R., Gobert O., Kaplan D. *Appl. Phys. B*, **99**, 7 (2010).
7. Minkovski N., Petrov G.I., Saltiel S.M., Albert O., Etchepare J. *J. Opt. Soc. Am. B*, **21**, 1659 (2004).
8. Naganuma K., Mogi K., Yamada H. *IEEE J. Quantum Electron.*, **25**, 1225 (1989).

9. Ginzburg V.N., Kochetkov A.A., Yakovlev I.V., Mironov S.Yu., Shaikin A.A., Khazanov E.A. *Quantum Electron.*, **46**, 106 (2016) [*Kvantovaya Elektron*., **46**, 106 (2016)].
10. Nibbering E.T.J., Franco M.A., Prade B.S., Grillon G., Chambaret J.-P., Mysyrowicz A. *J. Opt. Soc. Am. B*, **13**, 317 (1996).
11. Ferreiro J.J., de la Fuente R., Lopez-Lago E. *Opt. Lett*., **26**, 1025 (2001).
12. Anashkina E.A., Ginzburg V.N., Kochetkov A.A., Yakovlev I.V., Kim A.V., Khazanov E.A. *Sci. Rep.*, **6**, 33749 (2016).
13. Akhmanov S.A., Vysloukh V.A., Chirkin A.S. *Optics of Femtosecond Laser Pulses* (New York: Am. Inst. of Physics, 1992; Moscow: Nauka, 1988).
14. Gerchberg R.W., Saxton W.O. *Optik (Stuttgart)*, **35**, 237 (1972).
15. Rhodes M., Steinmeyer G., Trebino R. *Appl. Opt.*, **53**, D1 (2014).